Available online at www.sciencedirect.com

ScienceDirect

Ceramics International 39 (2013) 8995–9002

CERAMICS INTERNATIONAL

www.elsevier.com/locate/ceramint

Rod-like micelle templated synthesis of porous hydroxyapatite

Gunjan Verma[a,*], K.C. Barick[a], N. Manoj[a], A.K. Sahu[b], P.A. Hassan[a]

[a]Chemistry Division, Bhabha Atomic Research Centre, Mumbai 400085, India
[b]Glass and Advanced Materials Division, Bhabha Atomic Research Centre, Mumbai 400085, India

Received 7 February 2013; received in revised form 15 April 2013; accepted 28 April 2013
Available online 7 May 2013

Abstract

Use of macromolecular templates for controlling nanostructures of inorganic materials is an active area of research. In particular, oriented growth of hydroxyapatite in organic matrix is of great relevance to understand biomineralisation of bone and its potential biomedical applications. Natural bone being a composite of hydroxyapatite and collagen fibers, crystallization of hydroxyapatite in fibrous assemblies could mimic such biomineralisation. This motivated us to investigate the role of long rod-like micelles in modulating the structure of hydroxyapatite particles. In this article, we report the preparation of porous hydroxyapatite nanorods using rod-like micelles made up of a cationic surfactant cetyltrimethylammonium bromide (CTAB) and anionic hydrotrope sodium salicylate (SS) as a templating agent. The successful formation of hydroxyapatite crystals is evident from XRD, FTIR, TGA, SEM and TEM analyses. It has been observed that large hydroxyapatite nanorods of diameter ~50 nm are formed in surfactant mediated synthesis, whereas irregular shaped nanoaggregates of hydroxyapatite are obtained in the absence of surfactant. A comparative study on the porosity of hydroxyapatite clearly shows that monomodal distribution of mesopores with a peak at ~30 nm in the absence of surfactant while bimodal distribution of mesopores having maxima at ~4 nm and ~45 nm appear in hydroxyapatite prepared in the presence of surfactant template.

Keywords: Porosity; Hydroxyapatite; Rod-like micelles; Surfactant; Template synthesis

1. Introduction

Hydroxyapatite, with the chemical formula $Ca_{10}(PO_4)_6(OH)_2$, is a biocompatible material that has been extensively studied and applied in a variety of fields due to its similarity with the mineral constituents of human bones and teeth [1,2]. Bone is a hybrid material composed of needle-shaped inorganic hydroxyapatite nanocrystals and organic collagen matrix. Its properties depend intimately on its nano-scale structures, which are dictated specifically by the collagen template. Synthetic hydroxyapatite is widely applied in biomedical engineering due to its excellent biocompatibility and bioactivity [3]. It is also used as a filler to replace amputated bone and in the reconstruction of damaged bones and tooth zones. Many prosthetic implants are coated with hydroxyapatite to promote bone growth in implant [4,5]. The textural properties of hydroxyapatite, such as pore size, pore volume, pore structure etc., are also very important in addition to their chemical composition and structure for bone-forming ability. The porous nature of biomaterials allows the in-growth of bone tissue to achieve full amalgamation with the living bones. Also the mesoporous structure makes it feasible to incorporate biologically active molecules such as drug, osteogenic agents etc. that can treat bone infection and diseases and promote bone tissue regeneration [6–10]. Significant research efforts have been devoted to synthesize hydroxyapatite with controllable properties and porous structure using various techniques such as the sol–gel method, hydrothermal reaction, precipitation method, mechano-chemical, emulsion technique, wet-chemical method as well as by using surfactants as templates [11–16]. Stupp and Braun suggested that some of the biomolecules such as proteins, glycoproteins, and polysaccharides control nucleation and growth of mineral phases and thus manipulate their microstructure and physical properties [17]. By using this concept, they synthesized apatite-based materials in aqueous solutions of organic macromolecules, including homopolymer poly(amino acids), low molar mass

*Corresponding author. Tel.: +91 22 25590288; fax: +91 22 25505151.
E-mail addresses: gunjanv@barc.gov.in, gunjangarg@yahoo.com (G. Verma).

0272-8842/$ - see front matter © 2013 Elsevier Ltd and Techna Group S.r.l. All rights reserved.
http://dx.doi.org/10.1016/j.ceramint.2013.04.100

peptides, and synthetic polyelectrolytes. Analogous to that of biomolecules, synthetic polymers and surfactant assemblies can also drastically change the morphology and porosity of materials imparting new functional properties to them and provide new processing methods for the formation of useful objects. The self-assembly of surfactants by creating hydrophobic and hydrophilic structured domains provides an opportunity to use these systems as media for the synthesis of materials with unique properties. Recently, surfactant assemblies have been employed as templates for the synthesis of nanostructured hydroxyapatite particles. Both ionic and nonionic surfactant assemblies as well as block co-polymers have been attempted to tune the microstructure of hydroxyapatite particles [18–24].

Though, anisotropic and mesoporous structures formed by incorporation of surfactants in reaction medium are reported, true templating of micelle structure has not yet been proved. This motivated us to investigate the role of long rod-like micelles in modulating the structure of hydroxyapatite particles. Moreover, a detailed comparison of morphology and porosity behavior of hydroxyapatite prepared in the presence and absence of template has not been demonstrated to the full extent. The focus of the present work is to show the role of rod-like micelle templates composed of cationic surfactant and anionic hydrotrope in tuning the nanostructures of hydroxyapatite. It is anticipated that such templates will closely resemble the biomineralisation process in bone, which is a composite of hydroxyapatite and collagen fibers. Addition of organic hydrotropes (sodium salicylate, p-toluene sulphonates etc.) to cationic surfactant solution offers a novel way to create such rod-like micelles [25–27], which could be explored as a template for material synthesis.

Herein, we report the synthesis and characterization of hydroxyapatite nanoparticles using rod-like micelles of a cationic surfactant, cetyltrimethylammonim bromide (CTAB) and anionic hydrotrope, sodium salicylate (SS) as a templating agent and the comparison of its morphology and porosity behavior with respect to the hydroxyapatite prepared in the absence of any template under similar experimental conditions. To the best of our knowledge, this is the first study in which micelles composed of surfactant and hydrotrope have been utilized as a template for the synthesis of hydroxyapatite.

2. Material and methods

2.1. Chemicals

In this study, calcium nitrate ($Ca(NO_3)_2 \cdot 4H_2O$), di-sodium hydrogen phosphate (Na_2HPO_4) and cetyltrimethylammoinium bromide (CTAB) were obtained from S. D. Fine Chem. Ltd., Mumbai, India. Sodium salicylate (SS) and sodium hydroxide (NaOH) were purchased from Fluka Chemie, Buchs, Switzerland and BDH AnalaR®, E. Merck (India) Ltd., Mumbai, India, respectively. All chemicals were used as received. The nanopure water from a Millipore—Milli Q system (resistivity ~18 MΩ cm) was used to prepare aqueous solutions.

2.2. Synthesis of hydroxyapatite powders

We have prepared hydroxyapatite by precipitation followed by reflux [19]. In a typical synthesis of hydroxyapatite, 1.70 g of Na_2HPO_4 was dissolved in 100 ml of Milli Q water and pH was adjusted to 11.5 using 1 M NaOH solution. Then 4.72 g of $Ca(NO_3)_2.4\,H_2O$ was dissolved in 60 ml of Milli Q water and added dropwise to Na_2HPO_4 solution under stirring. The prepared milky suspension was refluxed at 100 °C for 2 h. The molar ratio of Ca/P was kept at 1.67 as in hydroxyapatite. The obtained precipitate was washed with Milli Q water by repeated centrifugation (at 8000 rpm for 10 min) and redispersion in water. The obtained precipitate was dried in an oven at 100 °C for 8 h and further calcined in a furnace at 550 °C for 6 h to obtain white powder of hydroxyapatite. For preparation of hydroxyapatite using surfactant as a template (HAp–CTAB–SS), 4.37 g of CTAB (120 mM) and 0.4 g of SS (25 mM) were dissolved in 100 ml Milli Q water along with 1.70 g Na_2HPO_4 followed by the same procedure as mentioned above. The obtained gel-like precipitate was separated and washed several times with water as mentioned earlier and then kept for drying in an oven at 100 °C for 8 h. It was further calcined in a furnace at 550 °C for 6 h for the removal of templates.

2.3. Characterization of micellar template

Dynamic light scattering (DLS) measurements were performed using a Malvern Autosizer 4800 (Malvern Instruments Ltd., UK) employing a 7132 digital correlator and APD detector. The light source was He–Ne laser operated at 632.8 nm with a maximum power output of 15 mW. All measurements were carried out at 30 °C using a circulating water bath. Cylindrical cell of 10 mm diameter was used in all of the light scattering experiments. The intensity of scattered light was measured five times for all the micellar solutions at a scattering angle of 130°. The autocorrelation function was obtained using a 192-channel photon correlator.

2.4. Characterization of hydroxyapatite powders

Phase analysis of the as-prepared (dried at 100 °C) and calcined hydroxyapatite (at 550 °C in air for 6 h) powders prepared in the presence (HAp–CTAB–SS) as well as in the absence (HAp) of surfactant template was carried out using powder X-ray diffraction (PXRD, Phillips PW1710) with CuKα radiation. Data were collected from 20° to 60° (2θ) with a step size of 0.02° and step time of 0.20 s. Fourier transform infrared spectra (FTIR, BOMEM MB series) were recorded in the range of 4000–450 cm^{-1} on powders prepared by the KBr-pellet technique. The weight ratio of KBr to sample was kept approximately 20:1. The thermal analysis of as-prepared samples was carried out between 30 °C and 700 °C in oxygen atmosphere by a TG-DTA instrument (Setaram Instrumentation, LABSYS 1600) at a heating rate of 10 °C/min. The morphological behavior of the as-prepared and heated (at 550 °C) samples was studied by using a scanning electron microscope (ATS 2100, SERON INC) and

transmission electron microscope (Philips CM 200). The surface area and porosity measurements were performed on samples heated at 550 °C by N_2 adsorption–desorption isotherm (Micromeritics ASAP 2020 surface area and porosity analyzer). The samples were thoroughly degassed prior to surface area and porosity measurements.

3. Results and discussion

3.1. Microstructure of micellar template

CTAB micelles in the presence of SS are known to form long rod-like micelles [25–27]. To understand the microstructure evolution in CTAB micelles with successive addition of hydrophobic salt SS in the presence of PO_4^{3-} ions, dynamic light scattering measurements were performed. To begin with, we used an equimolar solution of cationic surfactant CTAB (120 mM) and PO_4^{3-} ions (120 mM). This ensures that the amount of phosphate anions is sufficient to decorate the surface of micelles. To modulate the structure of micelles from spherical to rod-like the hydrotropic salt concentration (c_{ss}) was varied from 6 mM to 25 mM. The variation of apparent hydrodynamic diameter of template micelles obtained from the diffusion coefficient of the micelles using Stokes–Einstein relation [28] at different concentrations of SS is depicted in Fig. 1. In the absence of SS, the hydrodynamic diameter of CTAB/PO_4^{-3} micelles is ~5.5 nm, which is slightly more than the value expected (~4.3 nm) for small globular micelles of CTAB. According to Tanford's formula [29], the extended length of a cetyl chain of CTAB is 2.17 nm. Thus, the approximate diameter of the spherical micelles formed by CTAB molecules is expected to be ~4.3 nm as chain length of a surfactant molecule sets the maximum radius of the corresponding spherical micelle. This suggests the possibility of adsorption of phosphate anions on the surface of CTAB–SS micelles that leads to slight growth of the micelles due to the shielding of the surface charge. With successive addition of SS, there is a gradual increase in the average dimension of the micelles. At c_{ss} = 25 mM, the equivalent sphere diameter of the micelles is ~26 nm. However, it is unrealistic to have an isotropic spherical micelle having such a large value of diameter for CTAB molecules; since the maximum extended length of a cetyl chain is only 2.17 nm [29], any increase in radius beyond the length of the surfactant chain leads to the energetically unfavorable formation of void or water pool at the core of the micelle. It suggests that CTAB/PO_4^{-3} micelles are growing to long rod-like micelles upon addition of SS. We have employed these rod-like micellar templates of CTAB (120 mM) and SS (25 mM) for the synthesis of hydroxyapatite.

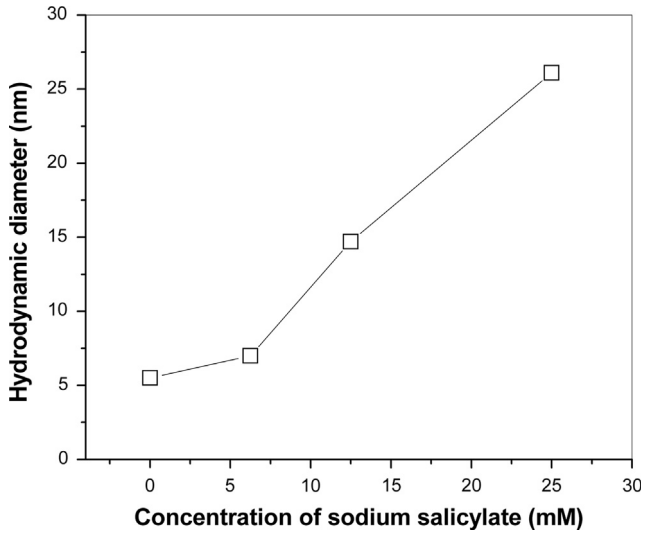

Fig. 1. Variation of apparent hydrodynamic diameter of CTAB/PO_4^{-3} micelles in the presence of different concentrations of SS at 30 °C.

3.2. Identification and microstructural characterization of the precipitate

3.2.1. Powder X-ray diffraction

The powder X-ray diffraction (PXRD) patterns of as-prepared and heated (550 °C) samples of HAp and HAp–CTAB–SS composites are shown in Fig. 2(a) and (b) respectively. PXRD analysis revealed the formation of single phase hexagonal hydroxyapatite (JCPDS files: 09-0432). It can be seen that all samples show the characteristic peaks of hydroxyapatite structure without any secondary phase formation. The appearance of broad peaks in PXRD suggests the formation of small size particles. Upon heating the samples at 550 °C, the crystal structure is retained.

3.2.2. Fourier transform infrared spectroscopy

FTIR studies were performed on HAp and HAp–CTAB–SS to investigate the composition of the samples. Fig. 3 shows FTIR spectra of the as-prepared and heated at 550 °C samples of HAp and HAp–CTAB–SS. From FTIR spectra, it could be inferred that all the stretching and bending vibrations of the PO_4^{3-} and OH^- functional groups remain in the same position in heated as well as non-heated samples of HAp and HAp–CTAB–SS. The weak shoulder at 960 cm^{-1} and strong broad band around 1030 cm^{-1} corresponds to ν_1 and ν_3 phosphate stretching modes while the strong peaks present at 565 and 605 cm^{-1} and the shoulder at 468 cm^{-1} indicate the presence of ν_4 and ν_2 phosphate bending modes [12]. The peaks present at 870 cm^{-1}, 1410 cm^{-1} and 1460 cm^{-1} in HAp and HAp–CTAB–SS as-prepared samples show the presence of CO_3^{-2} band positions [12,30]. This carbonate might come from the atmosphere carbon dioxide during sample preparation and would have incorporated into the HAp crystal structure. The carbonate peaks become less prominent in HAp as well as HAp–CTAB–SS samples upon heating at 550 °C. The bands appearing in the range of 2856–2970 cm^{-1} in HAp–CTAB–SS as-prepared sample could be ascribed to the bending and stretching modes of methylene groups (–CH_2), indicating the existence of surfactant chains within the hydroxyapatite particles. However, these vibrations are absent in

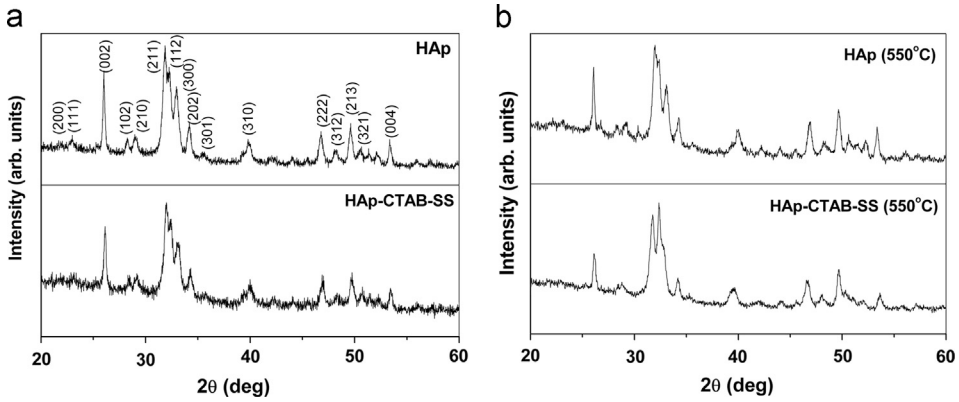

Fig. 2. PXRD patterns of (a) as-prepared HAp and HAp–CTAB–SS composite and (b) heated at 550 °C.

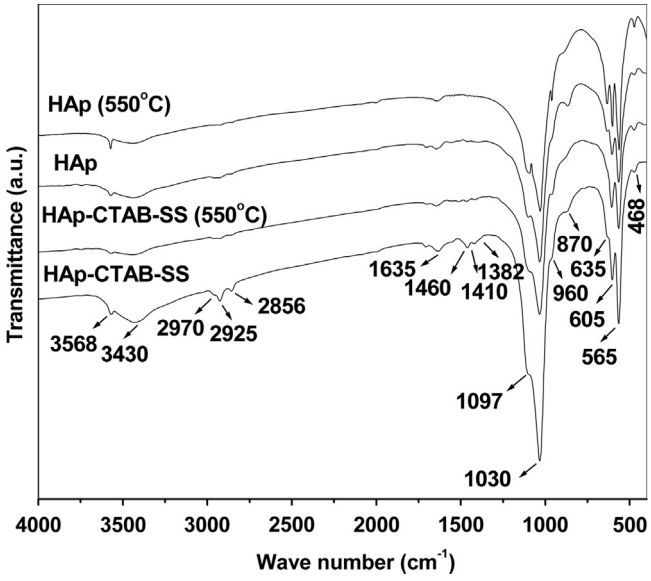

Fig. 3. FTIR spectra of as-prepared HAp and HAp–CTAB–SS composites, and HAp and HAp–CTAB–SS composites heated at 550 °C.

hydroxyapatite prepared in the absence of template and have almost disappeared in HAp–CTAB–SS annealed at 550 °C indicating the removal of template material. The weak peaks at 635 and 3568 cm^{-1} are ascribed to the stretching vibrations of the OH functional group. The broad peaks around 1635 and 3430 cm^{-1} reflecting the presence of water molecules are also observed. These results are in agreement with the previous reports on hydroxyapatite [30].

3.2.3. Thermal analysis

In order to investigate the chemical changes during heat treatment, the as-prepared samples of HAp and HAp–CTAB–SS were subjected to thermal studies. The thermogravimetric analysis (TGA) and its differential thermal analysis (DTA) trace are shown in Fig. 4(a) and (b) respectively. In both the samples, the weight loss observed up to 250 °C may be assigned to the removal of weakly bound (physically adsorbed) water molecules in the samples. In HAp–CTAB–SS, a major weight loss between 250 °C and 500 °C with sharp exothermic peak at about 300 °C was observed. This weight loss may be attributed to the removal of organic templates. Further, no significant weight loss was observed above 500 °C.

3.2.4. Electron microscopy

The microstructure evaluation of as-prepared HAp and HAp–CTAB–SS was carried out using scanning electron microscopy (SEM) and transmission electron microscopy (TEM). Fig. 5 shows the SEM micrographs of the samples synthesized in the (a) absence of surfactant (HAp) and (b) presence of CTAB and SS (HAp–CTAB–SS). The formation of irregular shaped aggregates comprised of numerous nanoparticles was evident from the SEM micrograph of hydroxyapatite prepared in the absence of template. On the other hand, an altogether different morphology showing the presence of self-assembled/ self-aggregated rod-like hydroxyapatite nanoparticulates was observed on addition of micellar templates during the synthesis of hydroxyapatite. Fig. 6 shows the SEM micrographs of (a) HAp and (b) HAp–CTAB–SS samples heated at 550 °C. No significant changes in the morphology of the samples could be observed upon heating. Further, the formation of rod-like hydroxyapatite having length of 100–500 nm and cross-section of ~50 nm is also evident from TEM images of as prepared HAp–CTAB–SS powder (Fig. 7). The selected area electron diffraction (SAED) pattern (inset of Fig. 7a) and HRTEM images (inset of Fig. 7b) indicate that all these synthetic nanorods were highly crystalline with a typical apatite structure. The crystal lattice planes were perfectly aligned and the lattice spacing was 0.28 nm, which can be assigned to the interplanar spacing of (211) planes for hexagonal hydroxyapatite.

The formation of rod-shaped hydroxyapatite nanoparticles in the presence of CTAB–SS is possibly due to the crystallization of hydroxyapatite nanoparticles on the surface of long rod-like micelles of CTAB and SS. There are other reports in which surfactant assemblies used as a template during synthesis have been shown to guide the morphology of the resulting hydroxyapatite. In the work of Shanti et al. [18], spherical particles of hydroxyapatite are formed in the presence of 4 mM cationic surfactant cetrimide. Similarly, Zhang and coworkers [21] have shown that in the presence of a nonionic surfactant, triton X-100, hydroxyapatite nanorods are formed which are

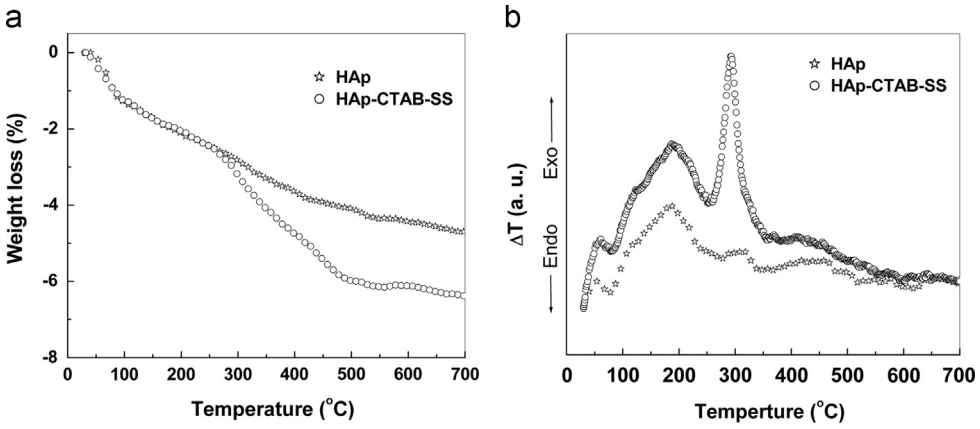

Fig. 4. TGA (a) and DTA (b) plots of pure HAp and HAp–CTAB–SS composites.

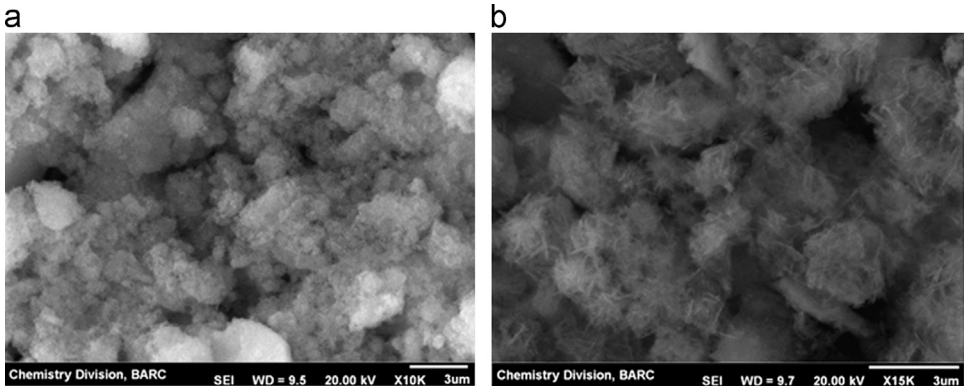

Fig. 5. SEM micrographs of as-prepared (a) HAp and (b) HAp–CTAB–SS composites.

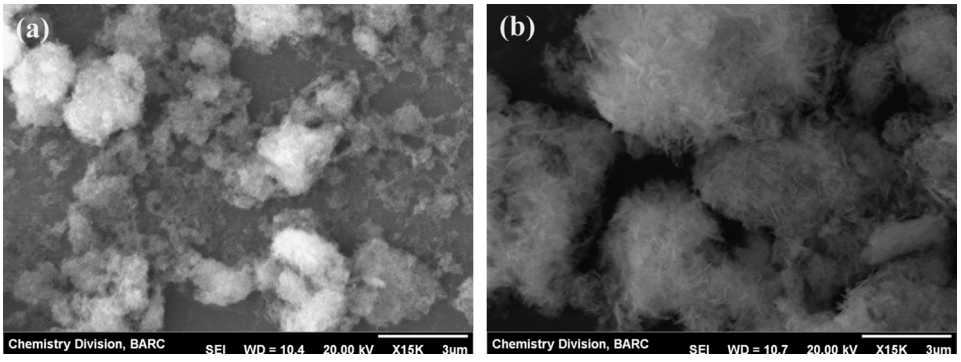

Fig. 6. SEM micrographs of (a) HAp and (b) HAp–CTAB–SS composites heated at 550 °C.

aligned and form big particles. According to them, the formation of well-aligned hydroxyapatite nanoparticles is presumably templated by triton X-100, which tends to form hexagonal phase. Yujie et al. have shown the role of dodecylphosphate micelles for the synthesis of nanocrystalline hydroxyapatite and demonstrated that the morphology as well as the surface area of the hydroxyapatite particles depends upon the concentration of the surfactant used [20].

In the present study, during synthesis of hydroxyapatite in the absence of surfactant template, PO_4^{3-} ions are randomly distributed in the solution. As a result of this, the addition of Ca^{2+} into the solution of PO_4^{3-} leads to precipitation of irregular size hydroxyapatite particles. On the other hand, in the presence of CTAB–SS micelles, the surface of the micelles is positively charged due to positive headgroup of CTAB. Upon addition of PO_4^{3-} to the solution of CTAB and SS, these negatively charged ions would have a tendency to bind to the surface of positively charged micelles due to the electrostatic attraction between them. In addition to this, both CTA^+ and PO_4^{3-} have tetrahedral structure, which could make them stereochemically compatible to interact with each other in an effective manner. Hence, possibly due to electrostatic attraction and complementary stereochemistry between the micelles and phosphate anions, an inorganic/organic network forms,

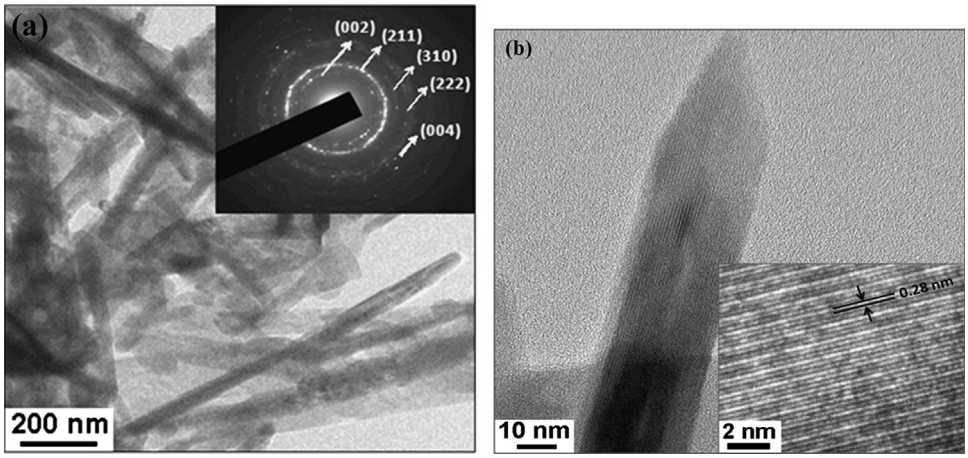

Fig. 7. (a) TEM image of as-prepared HAp–CTAB–SS (inset shows its selected area electron diffraction pattern) and (b) TEM image of a single HAp–CTAB–SS nanorod (inset shows its HRTEM image).

that might act as a nucleation center for the formation of hydroxyapatite. Upon drop-wise addition of Ca^{2+} solution into the network of CTAB–SS and PO_4^{3-} solution, co-precipitation of Ca^{2+} and PO_4^{3-} takes place on the hydrophilic surface of rod-like micelles. With the progress of the precipitation process more and more Ca^{2+} ions adsorb at the surface of micelle–phosphate ion network, which might lead to nanorod structures of HAp–CTAB–SS complex. In this way, the micelles might act as nucleating sites for the growth of hydroxyapatite nanorods. The plausible schematic of the formation of rod-shaped hydroxyapatite nanoparticles is shown in Scheme 1.

Apart from the controlled morphology, the use of templating agent in the synthesis of hydroxyapatite gives a porous structure. Porosity in hydroxyapatite is of great importance from a biomedical engineering point of view. Porous nature of biomaterial allows for the possibility of in-growth of natural bone, for bone cavity fillings, replacement of joints etc. and this also offers greater drug-loaded regions and larger surface to volume ratio. To evaluate the porous nature of hydroxyapatite prepared in the presence as well as in the absence of surfactant template, N_2 adsorption–desorption isotherm was performed on HAp and HAp–CTAB–SS samples heated at 550 °C. Upon heating the sample at 550 °C, the surfactant template burns out and creates the pores without disturbing the structure of the material as confirmed by PXRD, FTIR and SEM studies.

3.2.5. Porosity analysis

Fig. 8 shows typical N_2 adsorption–desorption isotherms for HAp and HAp–CTAB–SS samples (heated at 550 °C), which exhibit a type IV curve accompanied by a type H3 hysteresis loop [31]. Type IV isotherm corresponds to a mesoporous material. As can be seen from the curves, adsorption and desorption are not a reversible phenomenon which leads to the appearance of hysteresis between the curves of adsorption and desorption. Further, the presence of a pronounced hysteresis

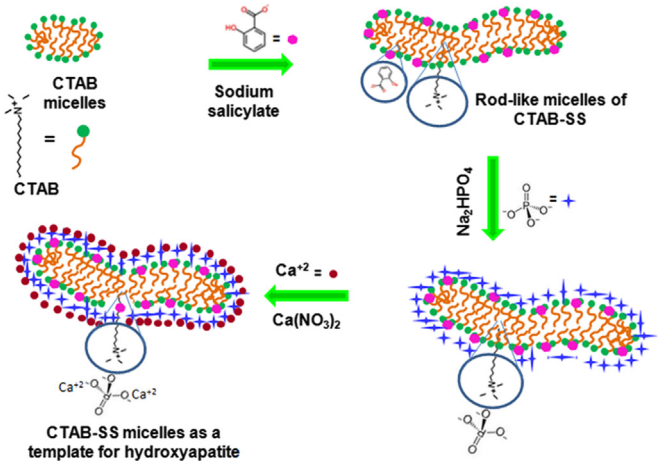

Scheme 1. A plausible schematic representation of the formation of hydroxyapatite nanorods using rod-like micellar templates.

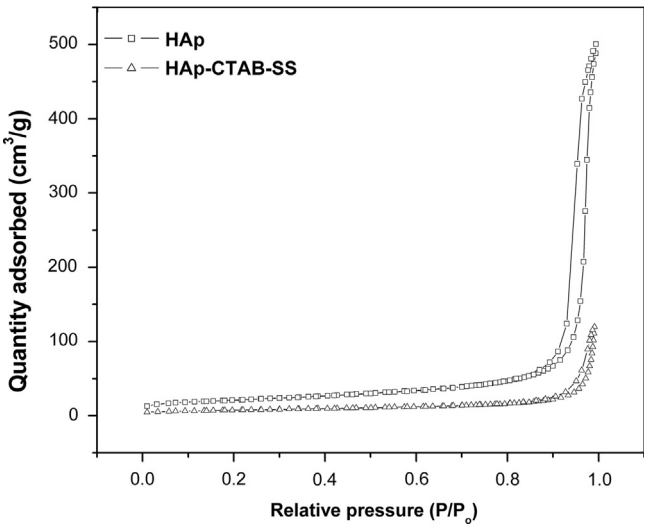

Fig. 8. N_2 gas adsorption–desorption isotherms of HAp and HAp–CTAB–SS samples.

loop in the isotherm curves is indicative of 3D intersection network of the mesopores [32] which goes well with the SEM observation. Due to the presence of large mesopores, the capillary condensation takes place at very high relative pressures and adsorption saturation is not significantly visible. It is also observed that the area of hysteresis loop decreases in the sample synthesized in the presence of CTAB and SS, i.e., HAp–CTAB–SS possibly due to the formation of larger size mesopores that results due to clustering of nanorods as observed in SEM and TEM. This in turn decreases the porous network and the area of hysteresis loop decreases.

The Brunauer–Emmett–Teller (BET) surface area plots of HAp and HAp–CTAB–SS samples correspond to the well known BET equation [33]. The specific BET surface areas of HAp and HAp–CTAB–SS were found to be 73.3 and 26.7 m^2/g, respectively, and the corresponding single-point total pore volumes at $P/P_o = 0.99$ are 0.774 and 0.185 cm^3/g, respectively. The observed variation in surface area and pore volume can be correlated to the agglomeration of the nanorods and formation of larger size mesopores in HAp–CTAB–SS, which in turn decrease the surface area and pore volume of the hydroxyapatite particles. Further analysis of the porous nature of the HAp and HAp–CTAB–SS was carried out by determining the pore size distribution of particles. The pore size calculation of samples for determination of the pores size distribution was performed on the desorption branch of the N_2 adsorption–desorption isotherm (since capillary condensation occurs at relatively higher pressure) by the Barrett–Joiner–Halenda (BJH) method [34]. The BJH desorption pore size distribution analysis confirmed the porous nature of both the samples. HAp particles show only monomodal distribution of mesopores whereas HAp–CTAB–SS particles show bimodal distribution of mesopores. The dV/dD pore volume vs. pore diameter curves (Fig. 9) clearly show broad distribution of mesopores with a peak at about 30 nm for HAp. However, HAp–CTAB–SS sample shows clear evidence for the generation (more than 50% population) of smaller size mesopores below 4 nm (inset of Fig. 9) along with a broad distribution of mesopores with a maximum at about 45 nm.

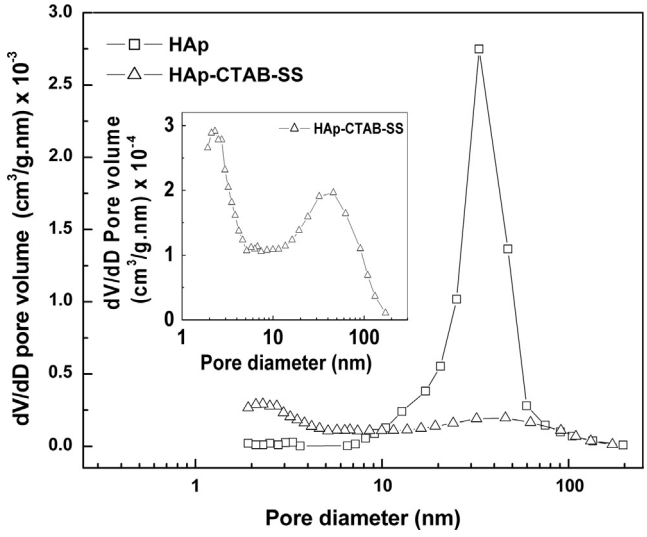

Fig. 9. *dV/dD* pore volume vs. pore diameter curves of HAp and HAp–CTAB–SS samples heated at 550 °C. Inset shows the *dV/dD* pore volume vs. pore diameter curve of HAp–CTAB–SS showing bimodal distribution of mesopores.

The appearance of smaller sized mesopores in HAp–CTAB–SS can be attributed to the presence of internal pores in the hydroxyapatite composites which originates due to the removal of CTAB–SS templates upon thermal treatment. The increase in the size and decreases in the population (pore volume) of the larger mesopores in the HAp–CTAB–SS system might possibly be due to the decrease in number of pores that might originate due to the clustering of nanorods in the HAp–CTAB–SS system. Thus, the present study demonstrates successful tuning of morphology and porosity behavior of hydroxyapatite by involving surfactant templates during the course of synthesis.

4. Conclusion

In summary, we have explored the role of rod-like micelles as templates for the synthesis of porous hydroxyapatite nanoparticles and compared its microstructure with that prepared in the absence of micelles. A remarkable difference in the morphology and porosity behavior could be observed in the hydroxyapatite prepared in the presence and absence of surfactant template. The SEM and TEM micrographs confirm the formation of hydroxyapatite nanorods (100–500 nm in length and ~50 nm in diameter) in the presence of surfactant template. On the other hand, random distribution of particles was observed in the absence of surfactant template. Moreover, HRTEM studies on rod-like hydroxyapatite particles suggest preferential growth of the crystals with the (2 1 1) planes arranged parallel to the rod axis. Such oriented growth of inorganic materials in the organic matrix is of great relevance to biomineralisation of bone and tissue engineering materials. The presence of bimodal distribution of mesopores was evident from porosity measurements in hydroxyapatite prepared in the presence of surfactant template while hydroxyapatite prepared in the absence of surfactant template shows monomodal distribution of mesopores. This difference in the morphology and porosity behavior may be due to the crystallization of hydroxyapatite nanoparticles on the surface of rod-like micelles of CTAB and SS. Specifically, the present study suggests that rod-like micelles composed of surfactant and hydrotrope could be promising soft templates for the crystallization of hydroxyapatite crystals. This could offer novel means of modulating the size, shape, orientation and nanostructures of hydroxyapatite particles. Moreover, the use of soft templates for the preparation of shape and size controlled hydroxyapatite nanorods might be useful for the development of biomimetic materials.

Acknowledgments

Authors are grateful to Dr. C. G. S. Pillai, Chemistry Division, BARC, for fruitful discussions and providing SEM facility.

References

[1] K.D. Groot, Bioceramics consisting of calcium phosphate salts, Biomaterials 1 (1980) 47–50.
[2] L.L. Hench, Bioceramics: from concept to clinic, Journal of the American Ceramic Society 74 (1991) 1487–1510.
[3] G. Grimandi, P. Weiss, F. Millot, G. Daculsi, In vitro evaluation of a new injectable calcium phosphate material, Journal of Biomedical Materials Research 39 (1998) 660–666.
[4] G.L. Lange, K. Donath, Interface between bone tissue and implants of solid hydroxyapatite or hydroxyapatite-coated titanium implants, Biomaterials 10 (1989) 121–125.
[5] B. Mavis, A.C. Tas, Dip coating of calcium hydroxyapatite on Ti–6Al—4V substrates, Journal of the American Ceramic Society 83 (2000) 989–991.
[6] W. Xia, J. Chang, Well-ordered mesoporous bioactive glasses (MBG): a promising bioactive drug delivery system, Journal of Controlled Release 110 (2006) 522–530.
[7] A. Simchi, E. Tamjid, F. Pishbin, A.R. Boccaccini, Recent progress in inorganic and composite coatings with bactericidal capability for orthopaedic applications, Nanomedicine: Nanotechnology, Biology and Medicine 7 (2011) 22–39.
[8] M. Vallet-Regí, F. Balas, D. Arcos, Mesoporous materials for drug delivery, Angewandte Chemie International Edition 46 (2007) 7548–7558.
[9] M. Betsiou, G. Bantsis, I. Zoi, C. Sikalidis, Adsorption and release of gemcitabine hydrochloride and oxaliplatin by hydroxyapatite, Ceramics International 38 (2012) 2719–2724.
[10] M. Colilla, M. Manzano, M. Vallet-Regí, Recent advances in ceramic implants as drug delivery systems for biomedical applications, International Journal of Nanomedicine 3 (2008) 403–414.
[11] A. Bigi, E. Boanini, K. Rubini, Hydroxyapatite gels and nanocrystals prepared through a sol–gel process, Journal of Solid State Chemistry 177 (2004) 3092–3098.
[12] J.B. Liu, X.Y. Ye, H. Wang, M.K. Zhu, B. Wang, H. Yan, The influence of pH and temperature on the morphology of hydroxyapatite synthesized by hydrothermal method, Ceramics International 29 (2003) 629–633.
[13] I. Mobasherpour, M.S. Heshajin, A. Kazemzadeh, M. Zakeri, Synthesis of nanocrystalline hydroxyapatite by using precipitation method, Journal of Alloys and Compounds 430 (2007) 330–333.
[14] L. Cao, C. Zhang, J. Huang, Synthesis of hydroxyapatite nanoparticles in ultrasonic precipitation, Ceramics International 31 (2005) 1041–1044.
[15] G. Guo, Y. Sun, Z. Wang, H. Guo, Preparation of hydroxyapatite nanoparticles by reverse microemulsion, Ceramics International 31 (2005) 869–872.
[16] K. Donadel, M.C.M. Laranjeira, V.L. Goncalves, V.T. Favere, J.C. de Lima, L.H. Prates, Hydroxyapatites produced by wet-chemical methods, Journal of the American Ceramic Society 88 (2005) 2230–2235.
[17] S.I. Stupp, P.V. Braun, Molecular manipulation of microstructures: biomaterials, ceramics, and semiconductors, Science 277 (1997) 1242–1248.
[18] P.M.S.L. Shanthi, R.V. Mangalaraja, A.P. Uthirakumar, S. Velmathi, T. Balasubramanian, M. Ashok, Synthesis and characterization of porous shell-like nano hydroxyapatite using Cetrimide as template, Journal of Colloid and Interface Science 350 (2010) 39–43.
[19] J. Yao, W. Tjandra, Y.Z. Chen, K.C. Tam, J. Mab, B. Soh, Hydroxyapatite nanostructure material derived using cationic surfactant as a template, Journal of Materials Chemistry 13 (2003) 3053–3057.
[20] Y. Wu, S. Bose, Nanocrystalline hydroxyapatite: Micelle templated synthesis and characterization, Langmuir 21 (2005) 3232–3234.
[21] J. Zhang, D. Jiang, J. Zhang, Q. Lin, Z. Huang, Synthesis of organized hydroxyapatite (HA) using triton X-100, Ceramics International 36 (2010) 2441–2447.
[22] J.D. Chen, Y.J. Wang, K. Wei, S.H. Zhang, X.T. Shi, Self-organization of hydroxyapatite nanorods through oriented attachment, Biomaterials 28 (2007) 2275–2280.
[23] M. Uota, H. Arakawa, N. Kitamura, T. Yoshimura, J. Tanaka, T. Kijima, Synthesis of high surface area hydroxyapatite nanoparticles by mixed surfactant-mediated approach, Langmuir 21 (2005) 4724–4728.
[24] B. Pre´lot, T. Zemb, Calcium phosphate precipitation in catanionic templates, Materials Science and Engineering C 25 (2005) 553–559.
[25] G. Garg, P.A. Hassan, S.K. Kulshreshtha, Dynamic light scattering studies of rod-like micelles in dilute and semi-dilute regime, Colloids and Surfaces A: Physicochemical and Engineering Aspects 275 (2006) 161–167.
[26] P.A. Hassan, S.J. Candau, F. Kern, C. Manohar, Rheology of wormlike micelles with varying hydrophobicity of the counterion, Langmuir 14 (1998) 6025–6029.
[27] S.V.G. Menon, P.S. Goyal, B.A. Dasannacharya, S.K. Paranjpe, R.V. Mehta, R.V. Upadhyay, When does a living polymer live? — Case of CTAB/NaSal, Physica B 213–214 (1995) 604–606.
[28] B.J. Berne, R. Pecora, Dynamic Light Scattering, Wiley, New York, 1976.
[29] C. Tanford, The Hydrophobic Effect: Formation of Micelles and Biological Membranes, Wiley, New York, 1980.
[30] X. Xiao, R. Liu, C. Qiu, D. Zhu, F. Liu, Biomimetic synthesis of micrometer spherical hydroxyapatite with β-cyclodextrin as template, Materials Science and Engineering C 29 (2009) 785–790.
[31] K.S.W. Sing, D.H. Everett, R.A.W. Haul, L. Moscou, R.A. Pierotti, J. Rouquerol, T. Siemieniewska, Reporting physisorption data for gas/solid systems with special reference to the determination of surface area and porosity, Pure and Applied Chemistry 57 (1985) 603–619.
[32] S.J. Gregg, K.S.W. Sing, in: Adsorption, Surface Area and Porosity, second ed., Academic Press, London, 1982.
[33] J.A. Curran, T.W. Clyne, Porosity in plasma electrolytic oxide coatings, Acta Materialia 54 (2006) 1985–1993.
[34] J.C. Groen, L.A. Peffer, J. Perez-Rremirez, Pore size determination in modified micro- and mesoporous materials. Pitfalls and limitations in gas adsorption data analysis, Microporous and Mesoporous Materials 60 (2003) 1–17.